Supporting Information

Table S1. Hansen solubility parameters (HSP, δ_T) for P3HT and the solvents used in this work (where δ_D is the dispersive, δ_P is the polar and δ_H is the hydrogen bonding interactions of HSP).[1,2]

Sample	δ_D (MPa$^{1/2}$)	δ_P (MPa$^{1/2}$)	δ_H (MPa$^{1/2}$)	δ_T (MPa$^{1/2}$)
P3HT	18.3	3.8	4.3	18.8
CB	18.8	4.5	2.3	19.5
CF	17.8	3.1	5.7	18.9
AN	15.3	18.0	6.1	24.4
DCM	18.2	6.3	6.1	20.2

References

(1) A. Panchal, S. K. Behera, B. Nath and P. C. Ramamurthy, Influence of thin-film processing on the performance of organic field-effect transistors. *J. Appl. Phys.*, 2022, **132**, 055501.

(2) M. Roesing, J. Howell and D. Boucher, Solubility characteristics of poly(3-hexylthiophene). *J..Polym. Sci. Part B: Polym. Phys.*, 2017, **55**, 1075-1087.
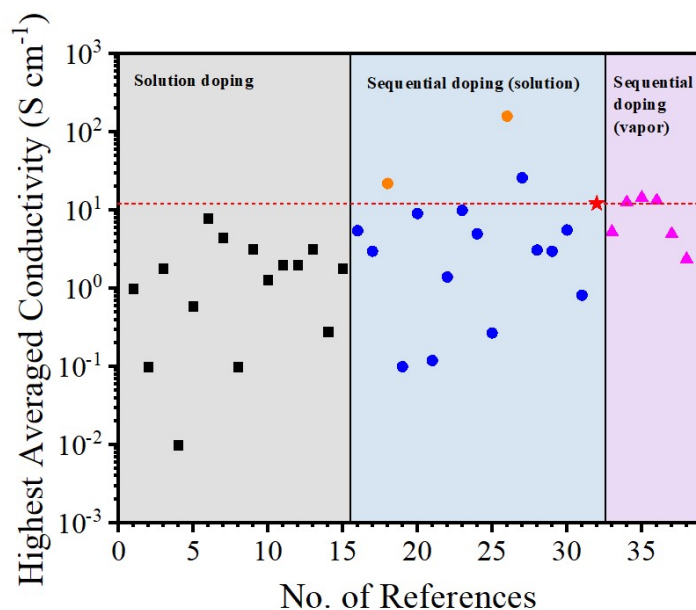
Figure S1. The highest conductivities of P3HT doped with F4TCNQ by solution doping or sequential doping (solution or vapor) from literatures. The data denoted by red star is the highest conductivity of our work. The orange circles denoted the conductivity of the oriented P3HT films.

References

(1) E. E. Aziz, A. Vollmer, S. Eisebitt, W. Eberhardt, P. Pingel, D. Neher and N. Koch, *Adv. Mater.*, 2007, **19**, 3257.

(2) K. Yim, G. L. Whiting, C. E. Murphy, J. J. M. Halls, J. H. Burroughes, R. H. Friend and J. Kim, *Adv. Mater.*, 2008, **20**, 3319-3324.

(3) D. T. Duong, C. Wang, E. Antono, M. F. Toney and A. Salleo, *Org. Electron.*, 2013, **14**, 1330-1336.

(4) D. T. Duong, H. Phan, D. Hanifi, P. S. Jo, T. Nguyen and A. Salleo, *Adv. Mater.*, 2014, **26**, 6069-6073.

(5) A. M. Glaudell, J. E. Cochran, S. N. Patel and M. L. Chabinyc, *Adv. Energy Mater.*, 2015, **5**, 1401072.

(6) I. E. Jacobs, E. W. Aasen, J. L. Oliveira, T. N. Fonseca, J. D. Roehling, J. Li, G. Zhang, M. P. Augustine, M. Mascal and A. J. Moulé, *J. Mater. Chem. C*, 2016, **4**, 3454-3466.

(7) L. Müller, D. Nanova, T. Glaser, S. Beck, A. Pucci, A. K. Kast, R. R. Schröder, E. Mankel, P. Pingel, D. Neher, W. Kowalsky and R. Lovrincic, *Chem. Mater.*, 2016, **28**, 4432-4439.

(8) D. Kiefer, L. Yu, E. Fransson, A. Gómez, D. Primetzhofer, A. Amassian, M. Campoy-Quiles and C. Müller, *Adv. Sci.*, 2017, **4**, 1600203.

(9) I. E. Jacobs, C. Cendra, T. F. Harrelson, Z. I. Bedolla Valdez, R. Faller, A. Salleo and A. J. Moulé, *Mater. Horiz.*, 2018, **5**, 655-660.

(10) H. Hase, K. O Neill, J. Frisch, A. Opitz, N. Koch and I. Salzmann, *J. Mater. Chem. C*, 2018, **122**, 25893-25899.

(11) B. Neelamraju, K. E. Watts, J. E. Pemberton and E. L. Ratcliff, *J. Phys. Chem. Lett.*, 2018, **9**, 6871-6877.

(12) K. E. Watts, B. Neelamraju, E. L. Ratcliff and J. E. Pemberton, *Chem. Mater.*, 2019, **31**, 6986-6994.

(13) M. P. Gordon, S. A. Gregory, J. P. Wooding, S. Ye, G. M. Su, D. S. Seferos, M. D. Losego, J. J. Urban, S. K. Yee and A. K. Menon, *Appl. Phys. Lett.*, 2021, **118**, 233301.

(14) C. E. Tait, A. Reckwitz, M. Arvind, D. Neher, R. Bittl and J. Behrends, *Phys. Chem. Chem. Phys.*, 2021, **23**, 13827-13841.

(15) Z. Liao, S. Wang, C. Gao and L. Wang, *Compos. Commun.*, 2022, **34**, 101255.

(16) D. T. Scholes, S. A. Hawks, P. Y. Yee, H. Wu, J. R. Lindemuth, S. H. Tolbert and B. J. Schwartz, *J. Phys. Chem. Lett.*, 2015, **6**, 4786-4793.

(17) I. E. Jacobs, E. W. Aasen, J. L. Oliveira, T. N. Fonseca, J. D. Roehling, J. Li, G. Zhang, M. P. Augustine, M. Mascal and A. J. Moulé, *J. Mater. Chem. C*, 2016, **4**, 3454-3466.

(18) M. P. Gordon, S. A. Gregory, J. P. Wooding, S. Ye, G. M. Su, D. S. Seferos, M. D. Losego, J. J. Urban, S. K. Yee and A. K. Menon, *Appl. Phys. Lett.*, 2021, **118**, 233301.

(19) A. R. Chew, R. Ghosh, Z. Shang, F. C. Spano and A. Salleo, *J. Phys. Chem. Lett.*, 2017, **8**, 4974-4980.

(20) D. T. Scholes, P. Y. Yee, J. R. Lindemuth, H. Kang, J. Onorato, R. Ghosh, C. K.

Luscombe, F. C. Spano, S. H. Tolbert and B. J. Schwartz, *Adv. Funct. Mater.*, 2017, **27**, 1702654.

(21) K. Tang, F. M. Mcfarland, S. Travis, J. Lim, J. D. Azoulay and S. Guo, *Chem. Commun.*, 2018, **54**, 11925-11928.

(22) T. J. Aubry, J. C. Axtell, V. M. Basile, K. J. Winchell, J. R. Lindemuth, T. M. Porter, J. Y. Liu, A. N. Alexandrova, C. P. Kubiak, S. H. Tolbert, A. M. Spokoyny and B. J. Schwartz, *Adv. Mater.*, 2019, **31**, 1805647.

(23) H. Jang, J. Wagner, H. Li, Q. Zhang, T. Mukhopadhyaya and H. E. Katz, *J. Am. Chem. Soc.*, 2019, **141**, 4861-4869.

(24) M. T. Fontana, D. A. Stanfield, D. T. Scholes, K. J. Winchell, S. H. Tolbert and B. J. Schwartz, *J. Phys. Chem. C*, 2019, **123**, 22711-22724.

(25) K. Tang, L. Huang, J. Lim, T. Zaveri, J. D. Azoulay and S. Guo, *ACS Appl. Polym. Mater.*, 2019, **1**, 2943-2950.

(26) V. Untilova, T. Biskup, L. Biniek, V. Vijayakumar and M. Brinkmann, *Macromolecules*, 2020, **53**, 2441-2453.

(27) S. E. Yoon, Y. Kang, G. G. Jeon, D. Jeon, S. Y. Lee, S-J Ko, T. Kim, H. Seo, B-G. Kim and J. H. Kim, *Adv. Funct. Mater*. 2020, **30**, 2004598.

(28) P. A. Finn, I. E. Jacobs, J. Armitage, R. Wu, B. D. Paulsen, M. Freeley, M. Palma, J. Rivnay, H. Sirringhaus and C. B. Nielsen, *J. Mater. Chem. C*, 2020, **8**, 16216-16223.

(29) J. Li, H. Li, Z. Ren, S. Yan and X. Sun, *ACS Appl. Mater. Interfaces*, 2021, **13**, 2944-2951.

(30) D. A. Stanfield, Y. Wu, S. H. Tolbert and B. J. Schwartz, *Chem. Mater.*, 2021, **33**, 2343-2356.

(31) D. Derewjanko, D. Scheunemann, E. Järsvall, A. I. Hofmann, C. Müller and M. Kemerink, *Adv. Funct. Mater.*, 2022, **32**, 2112262.

(32) This work

(33) K. Kang, S. Watanabe, K. Broch, A. Sepe, A. Brown, I. Nasrallah, M. Nikolka, Z. P. Fei, M. Heeney, D. Matsumoto, K. Marumoto, H. Tanaka, S. Kuroda and H. Sirringhaus, *Nat. Mater.*, 2016, **15**, 896.

(34) J. Hynynen, D. Kiefer, L. Yu, R. Kroon, R. Munir, A. Amassian, M. Kemerink and C. Müller, *Macromolecules*, 2017, **50**, 8140-8148.

(35) J. Hynynen, D. Kiefer and C. Muller, *RSC Adv.*, 2018, **8**, 1593-1599.

(36) E. Lim, A. M. Glaudell, R. Miller and M. L. Chabinyc, *Adv. Electron. Mater.*, 2019, **5**, 1800915.

(37) M. T. Fontana, D. A. Stanfield, D. T. Scholes, K. J. Winchell, S. H. Tolbert and B. J. Schwartz, *J. Phys. Chem. C*, 2019, **123**, 22711-22724.

(38) M. F. Ditusa, G. L. Grocke, T. Ma and S. N. Patel, *Mol. Syst. Des. Eng.*, 2022, **7**, 788-797.
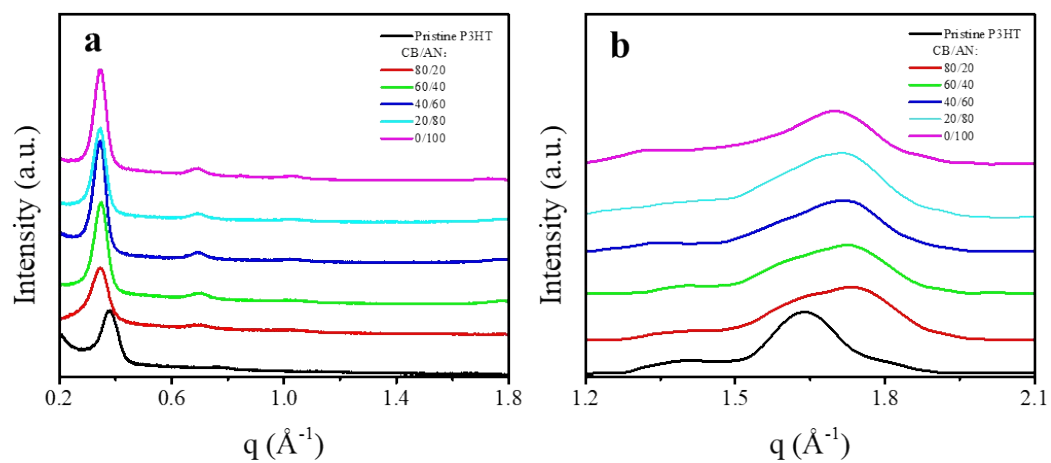
Figure S2. Thickness-normalized (a) out-of-plane and (b) in-plane GIXRD curves of spin-coated P3HT films doped with F4TCNQ from blend solvents with different ratios of CB and AN.
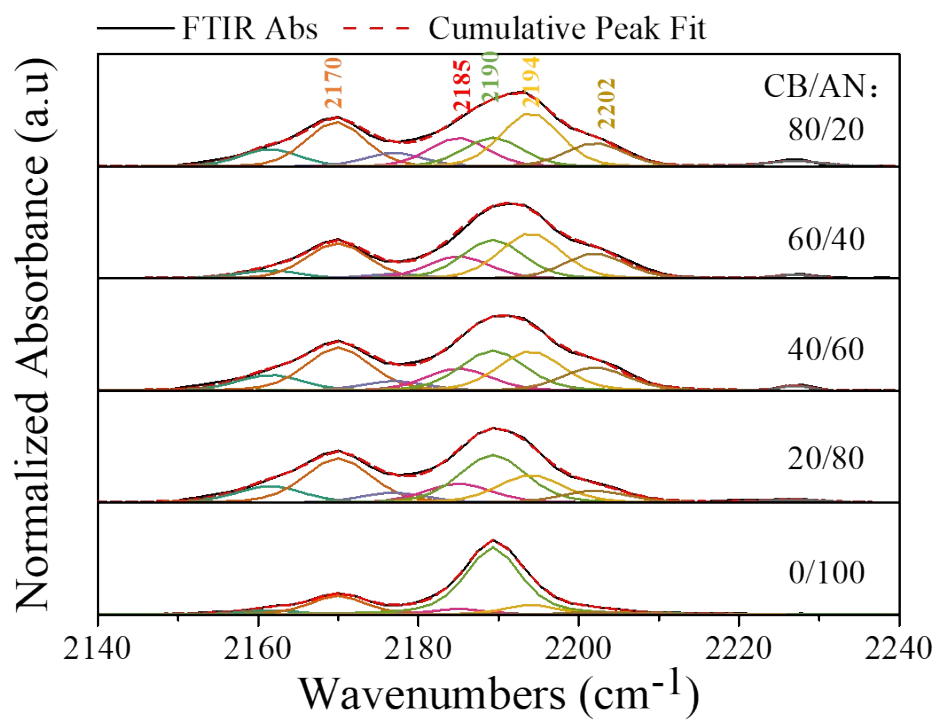
Figure S3. FTIR spectra subjected to spectral fitting for F4TCNQ-doped P3HT films in which the dopant is introduced sequentially from solvent blends containing various CB/AN ratios.
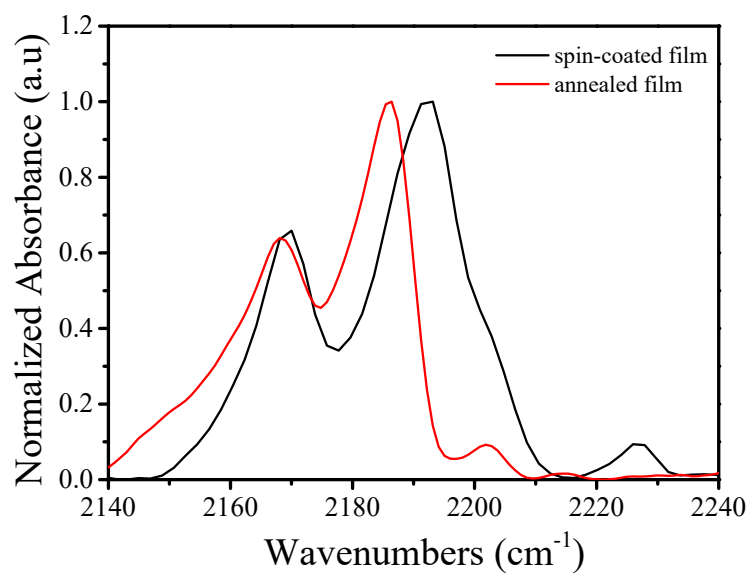
Figure S4. Normalized infrared absorbance of the C≡N stretching modes of F4TCNQ-doped spin-coated P3HT film and ODCB vapour annealed P3HT film in which the dopant is introduced sequentially from solvent blend containing CB/AN ratios of 80/20.
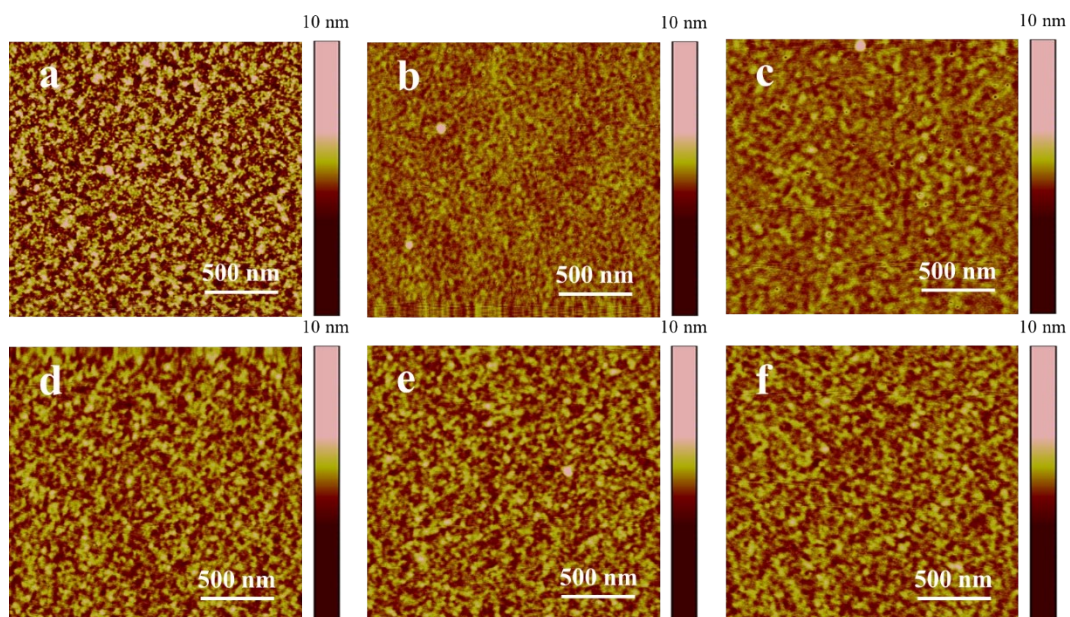
Figure S5. Tapping mode AFM height images of (a) spin-coated P3HT film and (b-f) spin-coated P3HT films in which the CB/AN solvent blend is introduced on the film surface and reside for 10 s before spin-coating. The CB/AN ratios in the solvent blends are: (b) 80/20, (c) 60/40, (d) 40/60, (e) 20/80 and (f) 0/100.

Hall effect measurements

For Hall effect measurements, four MoO_3-Ag electrodes (1.5 mm × 1.5 mm for each) are deposited through a shadow mask onto the surface of the doped polymer thin films using a vacuum coating system. The distance between two electrodes is 5 mm. Hall effect measurements are performed by physical property measurement system (PPMS, Quantum Design) using Van der Pauw geometries. From the linear fitting slope of resistivity to magnetic field, such as shown in Figure S6a-S6c, the Hall coefficient (R_H) can be obtained. The carrier density (n) and mobility (μ) can be calculated from $n = 1/eR_H$ and $\mu = \sigma/ne$, where e is the elementary charge and σ is the measured electrical conductivity by four probe method. [1,2]
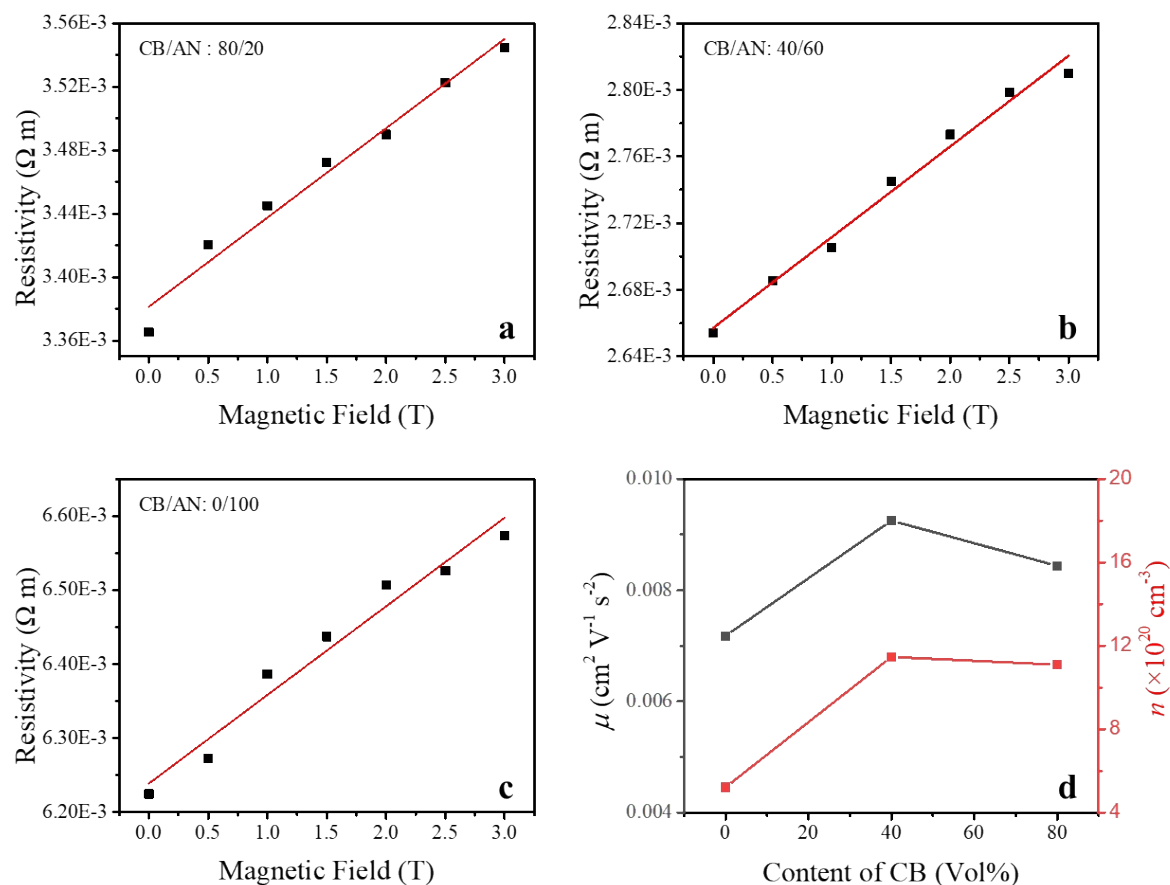
Figure S6. Linear fitting of resistivity to magnetic field for P3HT film doped from CB/AN blend solvent with the ration as (a) 80/20, (b) 40/60 and (c) 0/100. (d) The carrier density n and the mobility μ of doped P3HT films plotted against the volume fraction of CB in the doping solvent blend.

References

(1) Z. Chen, S. Qin, J. Jin, Y. Wang, Z. Li, J. Luo, H. Huang, L. Wang and D. Liu, Manipulating carrier concentration by self-assembled monolayers in thermoelectric polymer thin films. *ACS. Appl. Mater. Interfaces*, 2021, **13**, 32067-32074.

(2) Z. Liao, S. Wang, C. Gao, L. Wang, Combing chemical doping and thermal annealing to optimize the thermoelectric performance of the poly(3-hexylthiophene), *Compos. Commun*. 2002, **34**, 101255.
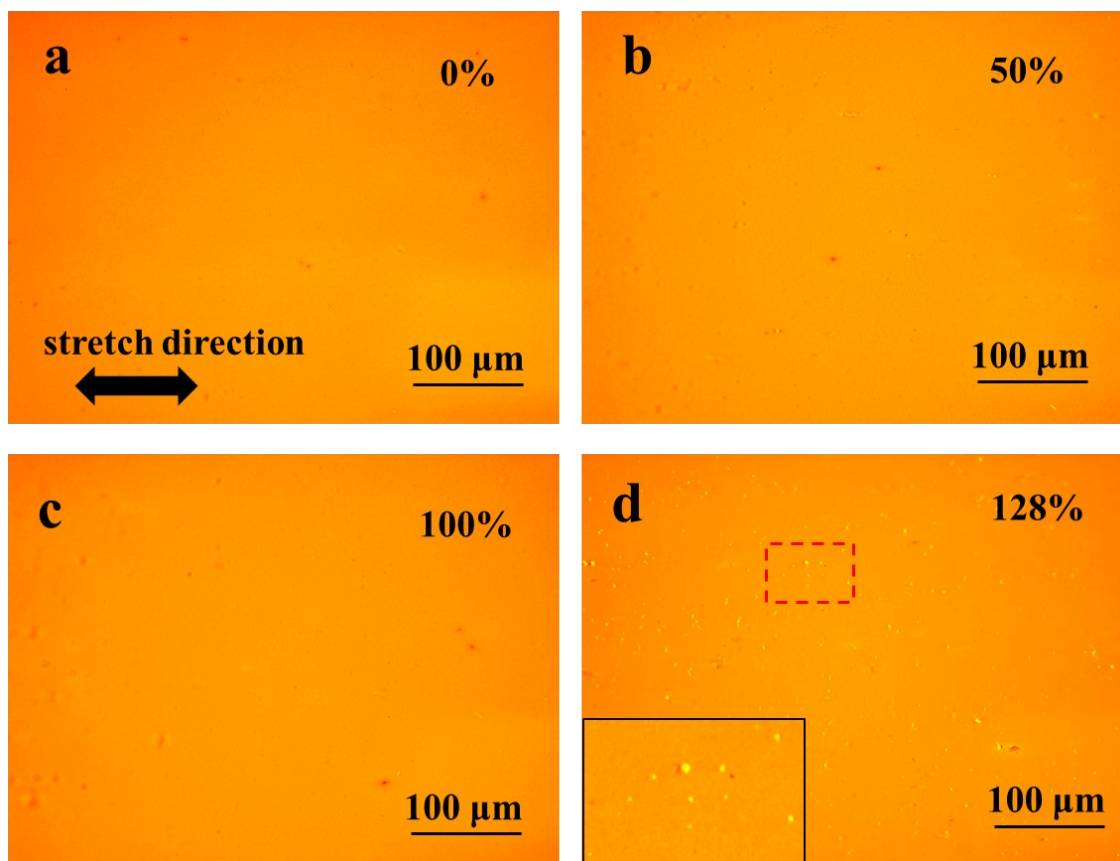
Figure S7. Optical microscopy images of an undoped P3HT film elongated under different strains. The specific strain is indicated in the upper right corner of the image; the double arrow in the (a) image indicates the stretching direction; the black border image in the bottom right corner is the modified image of that surrounded by the red dotted line in (d), and the same below.
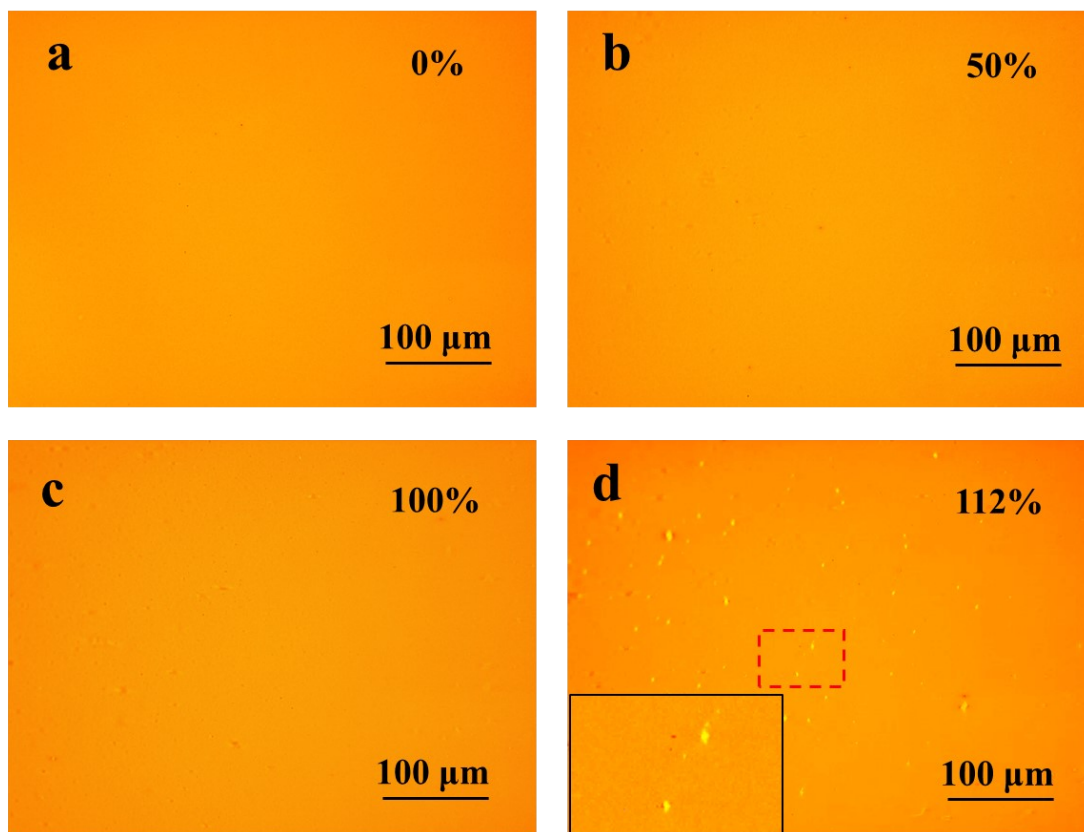
Figure S8. Optical microscopy images of F4TCNQ-doped spin-coated P3HT film elongated under different strains. The dopant is introduced sequentially from solvent blend with CB/AN as 80/20.
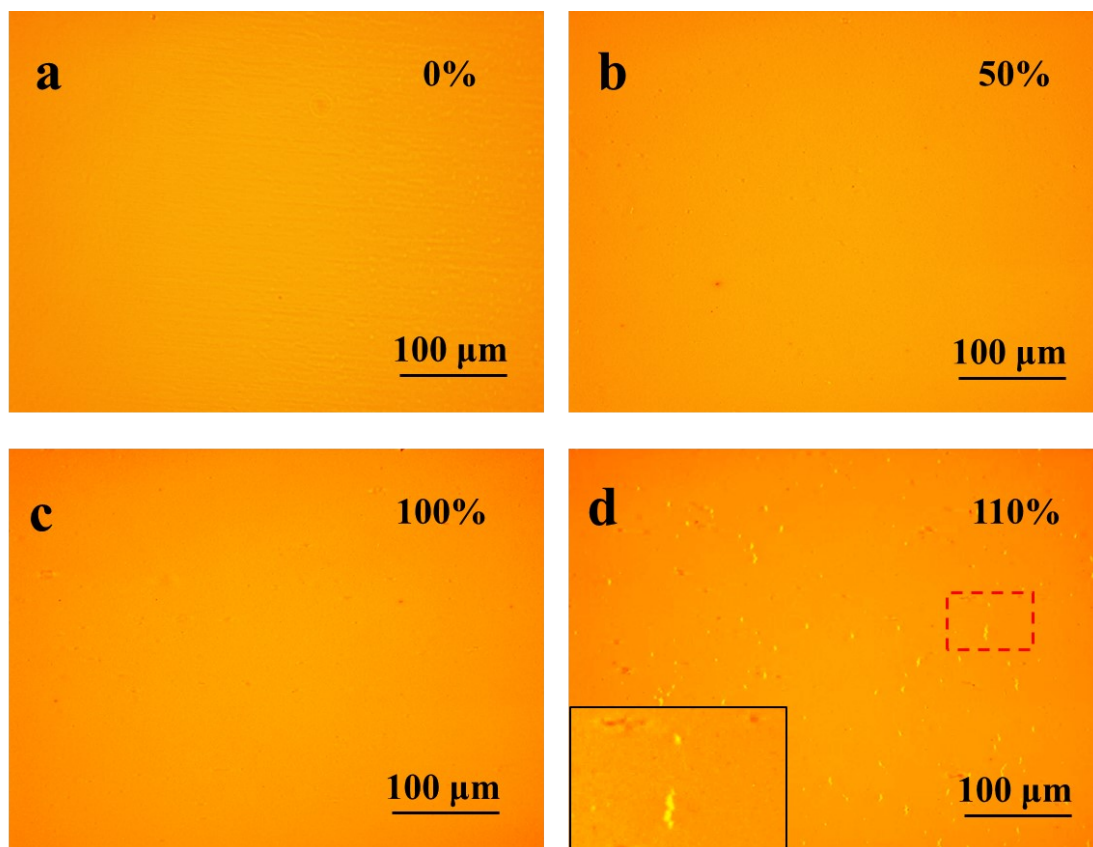
Figure S9. Optical microscopy images of F4TCNQ-doped spin-coated P3HT film elongated under different strains. The dopant is introduced sequentially from solvent blend with CB/AN as 60/40.
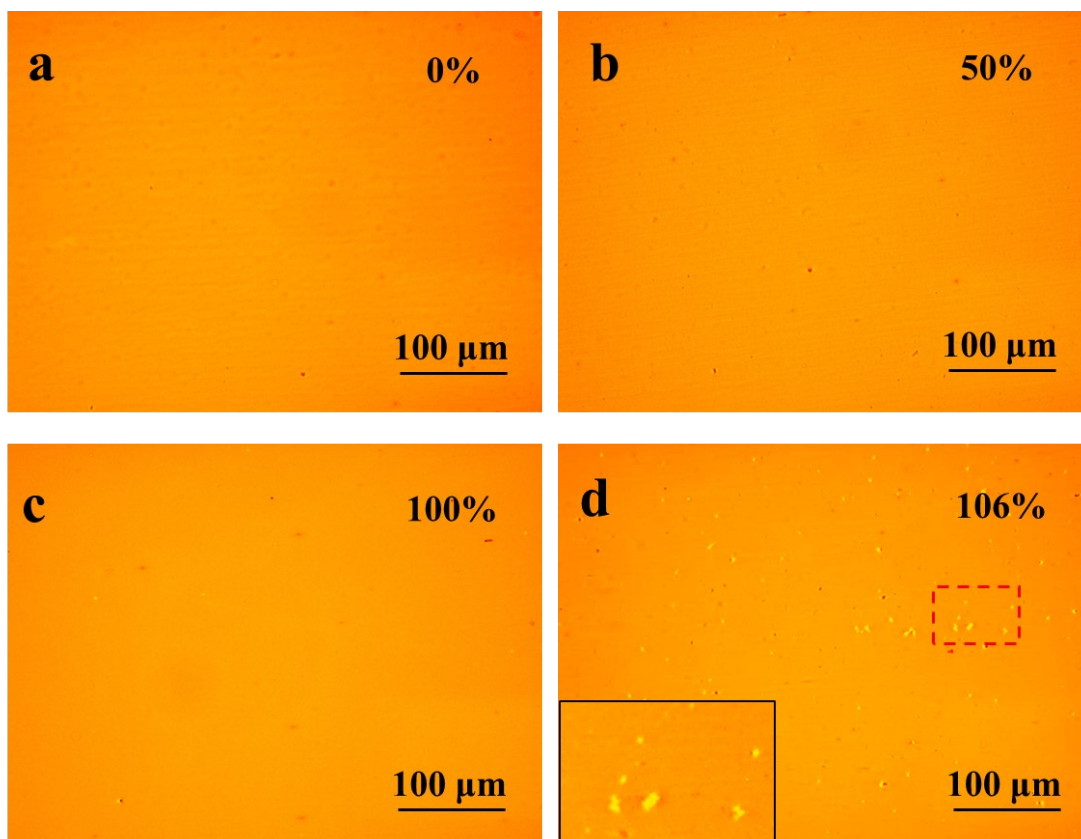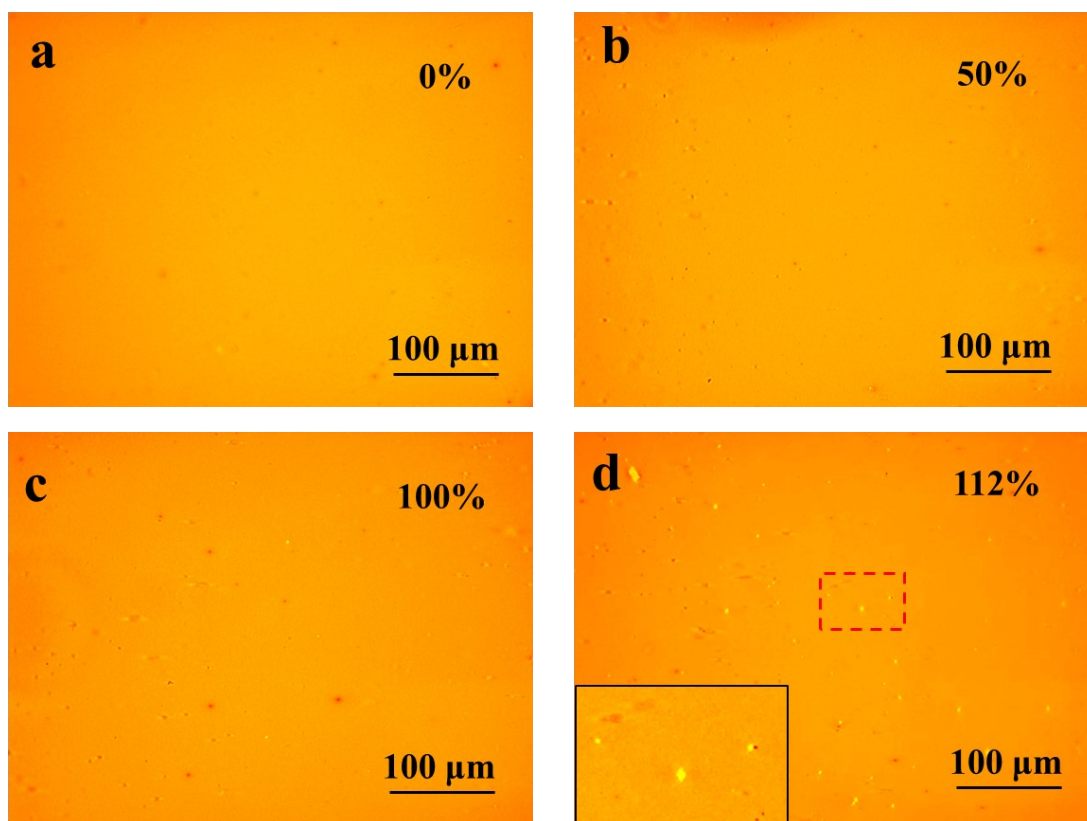
Figure S10. Optical microscopy images of F4TCNQ-doped spin-coated P3HT film elongated under different strains. The dopant is introduced sequentially from solvent blend with CB/AN as 40/60.

Figure S11. Optical microscopy images of F4TCNQ-doped spin-coated P3HT film elongated under different strains. The dopant is introduced sequentially from solvent blend with CB/AN as 20/80.
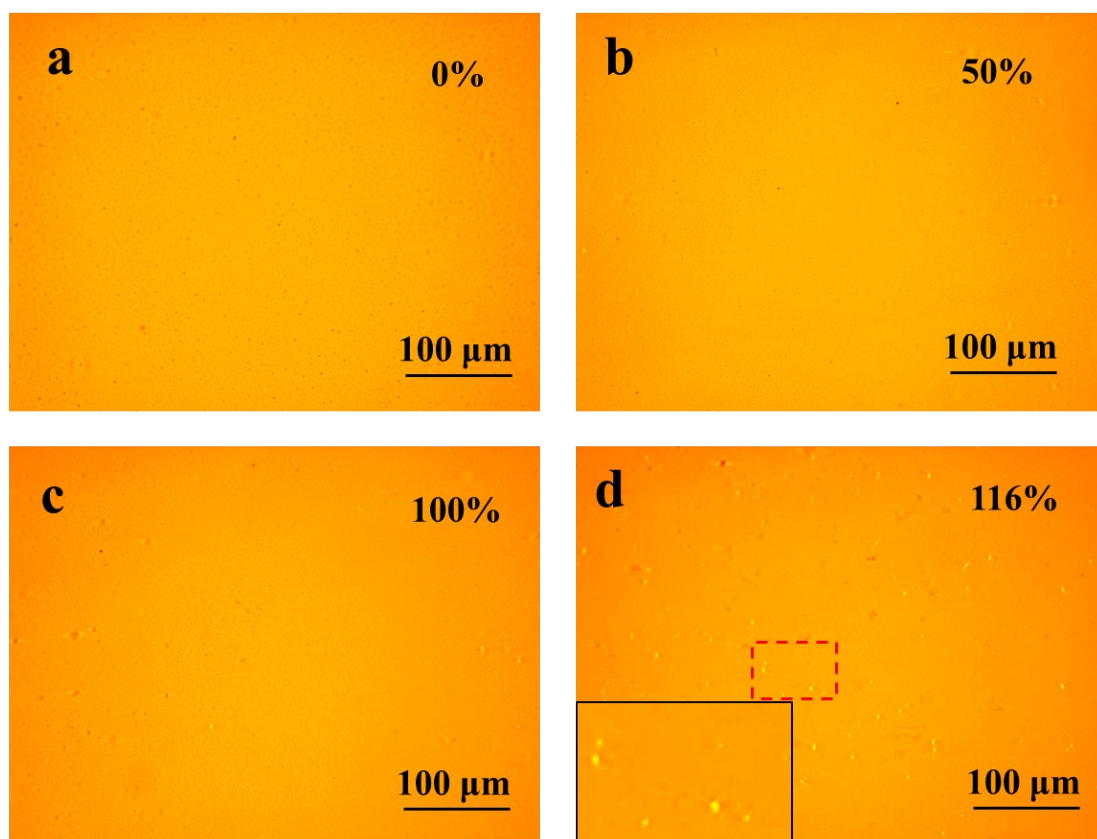
Figure S12. Optical microscopy images of F4TCNQ-doped spin-coated P3HT film elongated under different strains. The dopant is introduced sequentially from pure AN.
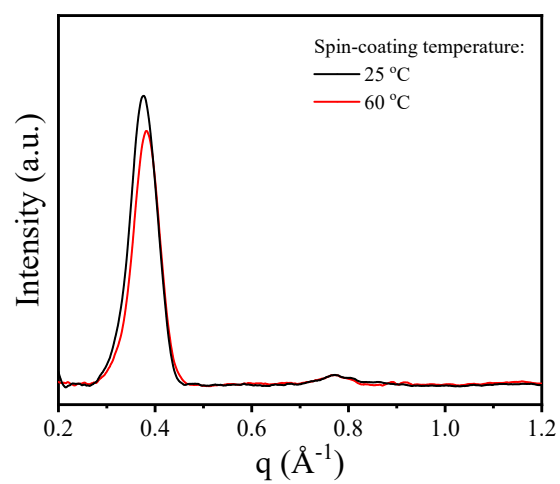
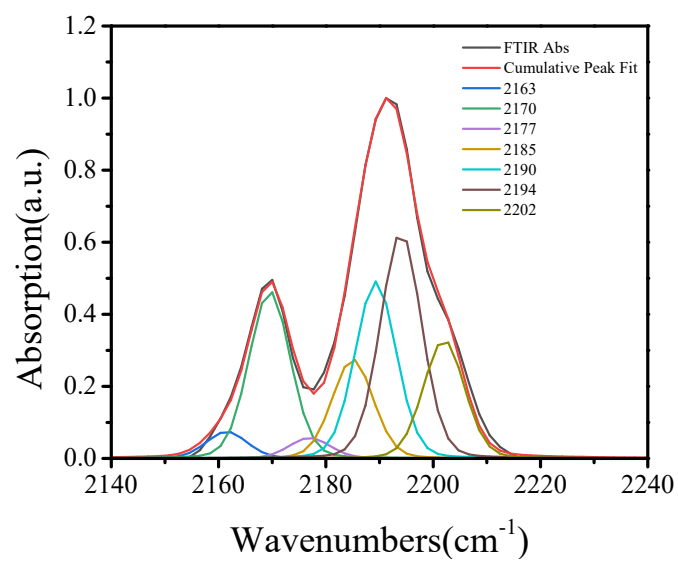Figure S13. GIXRD curves of P3HT films spin-coated from different temperatures.

Figure S14. Fitted FTIR spectra of P3HT-H film sequentially doped with F4TCNQ from a solvent blend with a CB/AN ratio of 20/80.